THE JOURNAL OF BIOLOGICAL CHEMISTRY
Vol. 278, No. 10, Issue of March 7, pp. 8452–8459, 2003
Printed in U.S.A.

Mouse MIM, a Tissue-specific Regulator of Cytoskeletal Dynamics, Interacts with ATP-Actin Monomers through Its C-terminal WH2 Domain*

Received for publication, November 27, 2002
Published, JBC Papers in Press, December 13, 2002, DOI 10.1074/jbc.M212113200

Pieta K. Mattila‡, Marjo Salminen§, Takashi Yamashiro§, and Pekka Lappalainen‡¶

From the Programs in ‡Cellular Biotechnology and §Developmental Biology, Institute of Biotechnology, P. O. Box 56, University of Helsinki, Helsinki 00014, Finland

The WH2 (WASP homology domain-2) is a small actin monomer-binding motif and is found in many proteins that regulate the actin cytoskeleton, including the β-thymosins, ciboulot, WASP, and verprolin/WIP (WASP-interacting protein). In sequence database searches we identified a novel mouse protein containing a WH2 domain in its C-terminal region. This mouse gene also shows strong sequence homology to human MIM (Missing in Metastasis), a cDNA fragment that is present in non-metastatic but absent in metastatic bladder cancer cell lines. Northern blot and *in situ* hybridizations show that MIM is strongly expressed in the developing neurons and skeletal and cardiac muscles in mouse embryos. In adult mice, the strongest expression of MIM mRNA is in liver, outer layers of the kidney, and in the Purkinje cells of the brain. Recombinant MIM protein interacts with actin monomers and inhibits actin filament nucleation *in vitro*. However, the MIM/ATP-G-actin complex can participate in actin filament assembly at the barbed end. MIM binds ATP-G-actin with a higher affinity (K_D = 0.06 μM) than ADP-G-actin (K_D = 0.3 μM) and inhibits the nucleotide exchange on actin monomers. Site-directed mutagenesis demonstrates that the actin monomer-binding site resides in the C-terminal WH2 domain of MIM. Overexpression of mouse MIM in NIH 3T3 cells results in the disappearance of actin stress fibers and appearance of abnormal actin filament structures. These data show that MIM is an ATP-G-actin binding protein that regulates cytoskeletal dynamics in specialized mammalian cell-types.

The actin cytoskeleton is central in a number of cellular processes such as motility, morphogenesis, cytokinesis, and endocytosis. The structure and dynamics of the actin cytoskeleton are spatially and temporally regulated by a large number of actin-binding proteins, whose own activities and localities are precisely regulated by various signaling pathways (1). Sequence and structural data on actin-binding proteins has revealed that many of these proteins interact with actin through a relatively small number of protein motifs. These include the calponin homology domain, the gelsolin homology domain, the actin-depolymerizing-factor homology domain, and the WASP homology 2 (WH2)[1] domain (for reviews see 2–5).

The WH2 domain is a small (~35 residue) protein motif that interacts only with monomeric actin (5, 6). WH2 domains are found in many regulators of actin dynamics, including β-thymosins and ciboulot, which bind actin monomers and regulate filament assembly. β-thymosins are actin monomer-sequestering proteins, whereas ciboulot promotes actin assembly at the barbed end of the filaments (7, 8). WH2 domains are also present in more complex proteins such as WASP/Scar, verprolin/WIP, and Srv2/CAP. These are multifunctional regulators of actin dynamics that link intracellular signaling pathways to actin dynamics (5). For example, WASP and Scar mediate signals from PIP_2 and the small GTPases Cdc42 and Rac to the actin cytoskeleton by inducing actin assembly through activation of the Arp2/3 complex (9–11). The WH2 domain is essential for the activity of WASP and Scar and is believed to facilitate the assembly of actin monomers to the newly formed filament ends (12, 13). Also verprolin/WIP proteins interact with actin monomers through their WH2 domains, but the biological role of their actin monomer-binding activity is still unclear (14).

We searched sequence databases for WH2 domain-containing proteins in mammals, *Drosophila melanogaster*, *Caenorhabditis elegans*, and *Saccharomyces cerevisiae*. In addition to the previously characterized WH2 domain proteins (β-thymosins, ciboulot, WASP, verprolin/WIP, Scar, Srv2/CAP) we identified several previously unknown WH2 domain-containing proteins (5). One of these proteins is particularly interesting because it is highly homologous to a human cDNA fragment named MIM (Missing In Metastasis) that was recently identified in a differential screen for mRNAs specifically expressed in non-metastatic bladder cancer cells (15).

We show that mouse MIM is an actin monomer-binding protein that efficiently inhibits the nucleotide exchange on actin monomers and actin filament nucleation *in vitro*. The strong actin-modulating activities reside in the C-terminal WH2 domain of MIM. We found that MIM is strongly expressed in the developing heart, skeletal muscle, and central nervous system. In adult mouse tissues, strong expression levels are detected in liver and in certain regions of brain and kidney. Overexpression of MIM results in the disappearance of stress fibers and formation of abnormal F-actin structures in NIH

* This study was supported by grants from the Academy of Finland, Biocentrum Helsinki, Sigrid Jusélius Foundation, and the European Molecular Biology Organization (EMBO) Young Investigator Program (to P. L.). The costs of publication of this article were defrayed in part by the payment of page charges. This article must therefore be hereby marked "*advertisement*" in accordance with 18 U.S.C. Section 1734 solely to indicate this fact.

The nucleotide sequence(s) reported in this paper has been submitted to the GenBank™/EBI Data Bank with accession number(s) AY214918.

¶ To whom correspondence should be addressed. Tel.: 358-9-19159499; Fax: 358-9-19159366; E-mail: pekka.lappalainen@helsinki.fi.

[1] The abbreviations used are: WH2, WASP homology domain-2; WASP, Wiscott-Aldrich syndrome protein; WIP, WASP-interacting protein; CAP, cyclase-associated protein; EST, expressed sequence tag; GFP, green fluorescent protein; GST, glutathione-*S*-transferase; MIM, missing in metastasis protein; MIM-CT, C-terminal half of MIM protein; NBD, 7-chloro-4-nitrobenz-2-oxa-1,3-diazole; DTT, dithiothreitol.

3T3 cells, suggesting that MIM regulates the dynamics of the actin monomer pool in specialized mammalian cells.

EXPERIMENTAL PROCEDURES

Plasmid Construction and Site-directed Mutagenesis—A DNA fragment corresponding to the full-length mouse MIM cDNA was amplified from I.M.A.G.E. Consortium mouse EST clone plasmid ID:5101888 (UK HGMP Resource Centre). The C-terminal half of mouse MIM was amplified from mouse E10 cDNA and I.M.A.G.E. Consortium mouse EST clone plasmid ID:2648606. Two different splice variants were obtained (see Fig. 1A), from which the shorter and more abundant form was used for the biochemical studies and is referred as MIM-CT in the text. The oligonucleotides used in the amplification of the full-length mouse MIM created *Bam*HI and *Hin*dIII sites and the oligonucleotides used in the amplification of MIM-CT created *Nco*I and *Hin*dIII sites at the 5′ and 3′ ends of the PCR fragment. These fragments were digested and ligated into the pGAT2 vector (16) to create plasmids pPL149 (full-length mouse MIM) and pPL106 (MIM-CT). The site-directed mutation, which replaced lysines 746 and 747 into alanines and deleted the last 11 amino acids 749–759, was introduced into the MIM-CT by PCR, and the amplification product was cloned into *Nco*I-*Hin*dIII-digested pGAT2 vector to create a plasmid pPL141. For generation of *in situ* probes MIM-CT cDNA fragment was cloned into the *Bam*HI (5′)-*Hin*dIII (3′) sites of pBSIIKS to create a plasmid pPL139. The plasmids for overexpressing green fluorescence protein (GFP) fusions of MIM were constructed by cloning the full-length MIM cDNA into the *Xho*I-*Bam*HI sites of pEGFP-N1 and pEGFP-C1A (Clontech) to create plasmids pPL151 and pPL153.

Northern Blotting—A mouse MIM cDNA probe was prepared from the plasmid pPL106 as described for mouse twinfilin (17). The MIM-CT cDNA probe was then hybridized to commercial mouse multiple tissue and mouse embryo Northern blots (Clontech) according to the manufacturer's instructions. The Northern blot filters were exposed on a phosphorimaging screen overnight. β-Actin controls were used to ensure equal amounts of RNA in each lane.

Radioactive in Situ Hybridizations—The antisense probe was obtained by linearizing the plasmid pPL139 with *Bam*HI and transcribing it with T3 RNA polymerase. For the sense probe *Hin*dIII and T7 RNA polymerase were used. The *in situ* hybridizations on the mouse tissue sections were performed using ^{35}S-UTP-labeled riboprobes as previously described (18).

Protein Expression and Purification—Mouse MIM-CT was expressed as a glutathione *S*-transferase (GST) fusion protein in *Escherichia coli* BL21 (DE3) cells under the control of T7 *lac* promoter. Cells were grown in 12 liters of Luria broth medium to an optical density of 0.5 at 600 nm, and the expression was induced with 0.2 mM isopropyl-β-D-1-thiogalactosidase. Cells were harvested 3 h after induction, washed with 180 ml of 20 mM Tris (pH 7.5), resuspended in 40 ml of phosphate-buffered saline, 0.2 mM phenylmethylsulfonyl fluoride, 1% Triton X-100, lysed by sonication, and centrifuged for 15 min at 15,000 × *g*. GST fusion proteins were enriched from the supernatant by glutathione-agarose beads (Sigma). The beads were then incubated overnight with thrombin (5 units/ml) at +4 °C to cleave MIM-CT away from GST. The beads were washed five times with 50 mM Tris-HCl (pH 7.5) and 150 mM $NaCl_2$, and the supernatant was diluted into 30 ml with 20 mM Tris-HCl (pH 7.5) and 25 mM NaCl. The solution was loaded onto an equilibrated Q-Sepharose High Performance Anion-exchange chromatography column (Amersham Biosciences) and eluted with a linear 0.025–1 M NaCl gradient. The peak fractions containing MIM-CT that eluted at ~0.35 M NaCl were pooled, and the buffer was exchanged to 10 mM Tris-HCl (pH 7.5) and 50 mM NaCl with a PD-10 desalting column (Amersham Biosciences). The protein solution was then concentrated in 10-kDa cutoff tubes (Centricon) into a final concentration of 100–200 μM divided into small aliquots, frozen in liquid N_2, and stored at −70 °C. Human platelet actin and pyrene-labeled actin (from rabbit skeletal muscle) were from Cytoskeleton Inc. Rabbit muscle actin was prepared from acetone powder as described in Pardee and Spudich (19).

Actin Monomer-binding Assay—We assayed the binding of MIM-CT to actin monomers by measuring the fluorescence of NBD-labeled G-actin. Rabbit muscle actin was labeled by NBD-Cl as described in Detmers *et al.* (20) and Weeds *et al.* (21). ADP-actin was prepared by incubating NBD-actin with hexokinase-agarose beads (Sigma) and glucose for 3 h at +4 °C (22). We used 0.2 μM actin and varied the concentration of MIM-CT from 0 to 3.2 μM. The reactions were carried out at room temperature in F-buffer (2 mM Tris, pH 8.0, 0.1 mM CaCl2, 0.1 mM DTT, 0.2 mM ADP or ATP, 0.5 mg/ml bovine serum albumin, 1 mM MgCl2, 0.1 M KCl). The normalized enhancement of fluorescence as determined by the equation

$$E = \frac{(F - F_0)}{(F_{max} - F_0)} \quad \text{(Eq. 1)}$$

was measured with BioLogic MOS250 fluorometer at each concentration of MIM-CT with an excitation at 482 nm and emission at 535 nm. The data were analyzed using SigmaPlot software and fitted using the following equation

$$E = \frac{1}{2}c + \frac{1}{2}z - \frac{1}{2}\sqrt{(c+z)\wedge 2 - 4z} \quad \text{(Eq. 2)}$$

where z and c are described in the two following equations.

$$z = \frac{[MIM]tot}{[Act]tot} \quad \text{(Eq. 3)}$$

$$c = 1 + \frac{K_d}{[Act]tot} \quad \text{(Eq. 4)}$$

Actin Filament Sedimentation Assays—Forty-μl aliquots of human platelet actin at desired concentration in G-buffer (20 mM Tris, pH 7.5, 0.2 mM ATP, 0.2 mM DTT, 0.2 mM $CaCl_2$) were polymerized for 30 min by the addition of 5 μl of 10× initiation mix (20 mM $MgCl_2$, 10 mM ATP, 1 M KCl). Five μl of MIM-CT (0, 10, 20, or 40 μM) in G-buffer was added to the actin filaments followed by a 30-min incubation. The actin filaments were sedimented by centrifuging at 217,000 × *g* for 30 min in a Beckman Optima MAX Ultracentrifuge and a TLA 100 rotor. All steps were performed at room temperature. Equal proportions of supernatant and pellet fractions were loaded onto 10% SDS-polyacrylamide gels; the gels were stained with Coomassie Blue and scanned with FluorS-Imager (Bio-Rad, Hercules, CA).

Pyrene Actin Filament Assembly Assays—We followed actin polymerization in the presence of MIM by determining the increase in the fluorescence of pyrene-labeled actin (Cytoskeleton). Three μM actin (1:5 pyrene-labeled rabbit muscle actin:human platelet actin) with 0, 0.75, or 3 μM MIM-CT or MIM-CTΔWH2 in G-buffer (5 mM Tris-HCl, pH 7.5, 0.2 mM ATP, 0.2 mM DTT, 0.2 mM $CaCl_2$) was polymerized by adding 1/10 reaction volumes of 10× initiation mix (20 mM $MgCl_2$, 10 mM ATP, 1 M KCl). Kinetics of actin filament assembly was followed by a BioLogic MOS-250 fluorescence spectrophotometer at an excitation wavelength of 365 nm and an emission wavelength of 407 nm. To examine the effect of MIM-CT for pointed end and barbed end filament assembly, gelsolin-actin seeds (10 nM) or phalloidin-stabilized actin seeds (0.4 μM) were added to a mixture of 3 μM actin and desired concentration (0–6 μM) of MIM-CT in F-buffer. The phalloidin-actin seeds were prepared as described (23),and gelsolin-actin seeds as described (24). The rate of actin filament assembly was monitored as described above.

Nucleotide Exchange Assay—The rate of nucleotide exchange was measured from the fluorescent signal provided by ϵ-ATP bound to G-actin. Human platelet actin was dialyzed against ϵ-ATP-G-buffer (20 mM Tris, pH 8.0, 1 mM DTT, 0.4 mM $CaCl_2$, 0.2 mM ϵ-ATP) overnight at +4 °C. An 80-μl mixture of ϵ-ATP-actin and MIM-CT was prepared in G-buffer with final concentrations of 0.5 μM for actin and 0, 0.5, 1, 1.5, 2, or 4 μM for MIM-CT. Twenty μl of 5 mM ATP was added to the mixture, and the reaction was immediately monitored by a BioLogic MOS-250 fluorescence spectrophotometer using an excitation wavelength of 360 nm and an emission wavelength of 410 nm.

Cell Culture and Immunofluorescence—NIH 3T3 cells were maintained in Dulbecco's modified Eagle's medium supplemented with 10% fetal bovine serum (Invitrogen), 2 mM L-glutamine, 100 units/ml penicillin, and 100 mg/ml streptomycin. Cells were transfected with 1.5 μg of the desired plasmid using the FuGENE6 transfection reagent (Roche Molecular Biochemicals) according to the manufacturer's instructions. Immunofluorescence was carried out as described in Vartiainen *et al.* (17). Tetramethylrhodamine B isothiocyanate-conjugated phalloidin (Molecular Probes) was used at a 1:400 dilution to visualize actin filaments.

Miscellaneous—SDS-PAGE was carried out by using the buffer system of Laemmli (25). Protein concentrations were determined with a Hewlett Packard 8452A diode array spectrophotometer by using the calculated extinction coefficients for mouse MIM-CT (ϵ_{280} = 17,780 M^{-1} cm^{-1}) and for actin ($\epsilon_{290-340}$ = 26,600 M^{-1} cm^{-1}). Protein concentrations were also estimated from Coomassie Blue-stained SDS-PAGE. Fluorescence-monitored urea denaturation assays were carried out as described in (26).

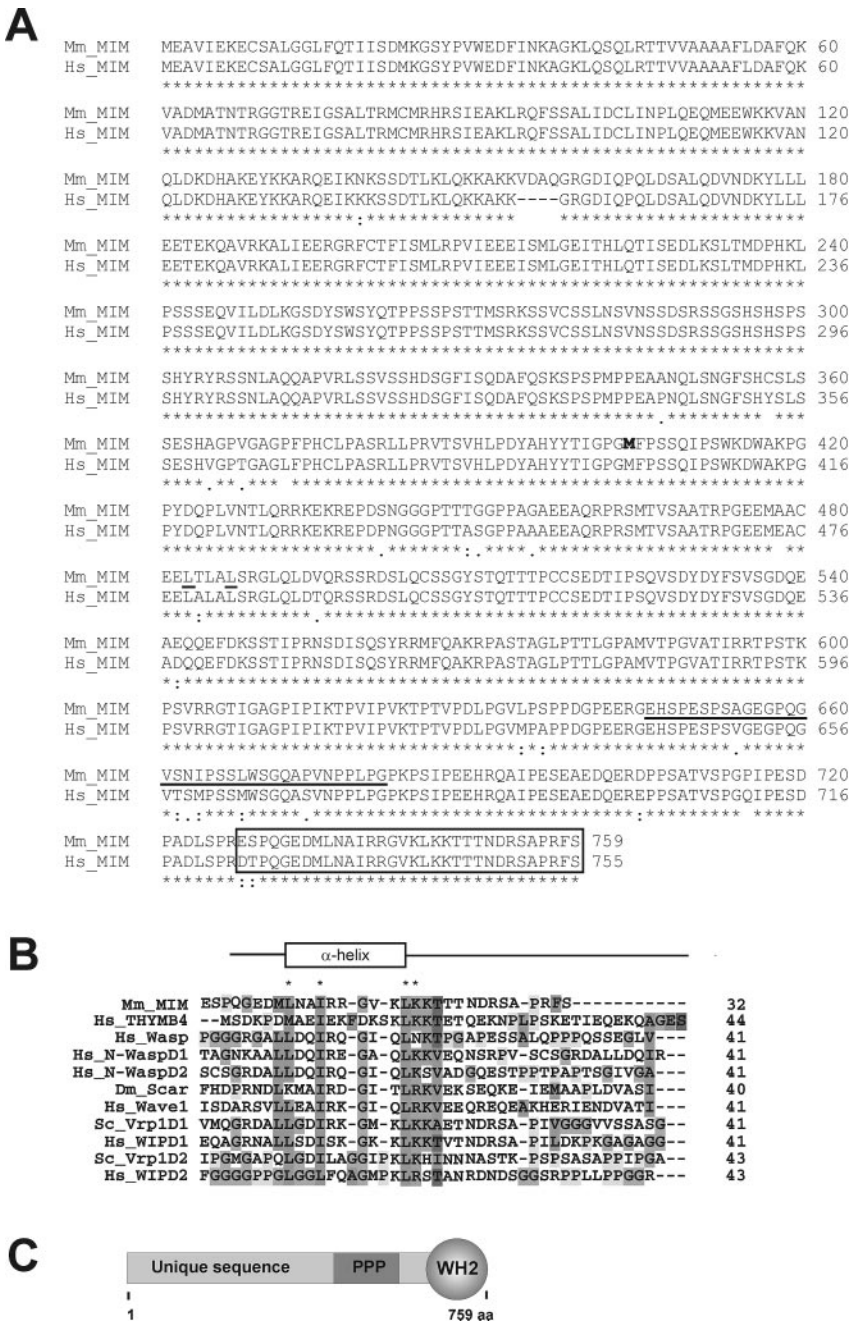

FIG. 1. **The sequences and domain structures of mouse and human MIMs.** *A*, an alignment of mouse (*Mm*) and human (*Hs*) MIM amino acid sequences. The WH2 domains in the C termini are boxed. Two splice variants were identified from mouse MIM. The longer variant corresponds to the sequence shown in the figure, whereas the shorter and more abundant variant lacks amino acids 646–681 (*underlined*) and contains Leu-to-Pro substitutions in residues 483 and 487 (*underlined*). The Met-404 residue that was used as a start codon for expressing the C-terminal half of MIM in *E. coli* is *bolded*. *B*, a multiple sequence alignment of the WH2 domains of mouse MIM, human thymosin-β4 (EMBL M17733), human WASP (TrEMBL AF115549), human N-WASP (TrEMBL D88460), human Scar1 (EMBL D87459), human WIP (TrEMBL AF031588), fly Scar (NCBI AAF53042), and yeast verprolin (SGD YLR337W). The *asterisks* indicate the residues that are essential for actin monomer-binding in thymosin-β4 (28). Furthermore, the position of an α-helix in the WH2 domain of thymosin-β4 in indicated above the sequence (37). *C*, a schematic representation of the domain structure of mouse MIM. The GenBank accession number for mouse MIM cDNA sequence is AY214918.

RESULTS

Identification of a Novel Mouse WH2 Domain Protein—In database searches for novel WH2 domain-containing proteins, we identified several independent mouse ESTs that encoded a putative protein with a C-terminal WH2 domain. A full-length sequence of the coding region of this cDNA was obtained by sequencing I.M.A.G.E. consortium mouse EST clone plasmid ID:5101888. The predicted protein is composed of 759 residues with an N-terminal sequence (MEAVI . . .). There is an in-frame stop codon 85 nucleotides upstream to the methionine (AUG) codon, and the nucleotides immediately 5′ to this AUG codon fulfill the rules for translational initiation sequences (27), suggesting that translation is initiated at this methionine. Our EST database searches and sequencing of PCR fragments from this mouse cDNA showed that a shorter form of this protein also exists. The shorter form lacks amino acids 646–681 and contains Leu-to-Pro substitutions at residues 483 and 487 (Fig. 1*A*). Because the nucleotide sequences of these two isoforms are otherwise identical, they are most likely splice variants of the same gene.

Our database searches revealed a human homologue that is 96% identical at the amino acid level. While the putative coding regions of the human and mouse cDNA clones were nearly identical at the nucleotide level, the regions 5′ from the putative translational initiation codons showed significantly lower homology. This provides further support that translation starts at this AUG codon. Interestingly, a region in the human cDNA is identical to an ~300-bp cDNA fragment that was recently identified by differential display as a gene that was specifically expressed in non-metastatic bladder cancer cells and consequently named MIM (15). Both mouse and human MIM contain a WH2 domain in their C termini (Fig. 1*A*). The residues that are important for actin monomer-binding in the WH2 domain of thymosin-β4 (28) are well conserved in human and murine MIM, suggesting that these proteins interact with monomeric actin (Fig. 1*B*). The human and mouse MIMs also contain a

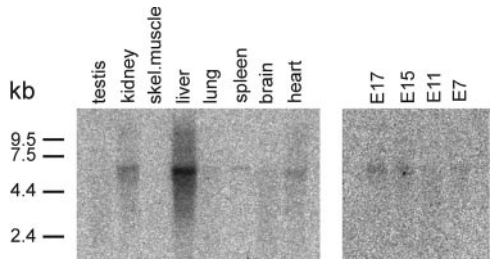

FIG. 2. **Northern blot analysis of MIM mRNA expression in adult mouse tissues (*left panel*) and embryogenesis (*right panel*).** The ~6-kb MIM mRNA is strongly expressed in the liver, in moderate amounts in the kidneys and heart, and at lower levels in lung, spleen, and brain. There is no detectable expression in skeletal muscle and testis. The relative levels of MIM mRNA increase during embryonic development.

proline-rich region but otherwise do not share any detectable sequence homology to other known proteins (Fig. 1*C*).

Expression of MIM in Mouse Embryos and Adult Mouse Tissues—To examine the expression patterns of MIM, we carried out Northern blot and *in situ* hybridization analyses on embryonic and adult mouse tissues. A multiple-tissue Northern blot analysis showed that MIM mRNA is expressed in several adult mouse tissues at variable levels (Fig. 2, *left panel*). Particularly strong expression was detected in liver. The kidney, heart, lung, spleen, and brain showed only moderate or weak expression of MIM mRNA. No expression could be detected in skeletal muscle and testis. A Northern blot analysis of mouse embryos at different stages showed that the relative MIM expression increases during development (Fig. 2, *right panel*). The MIM cDNA probe used in this study recognized only a single ~6-kb mRNA, indicating that the probe was specific. The two MIM splice variants are very close to each other in size, and therefore cannot be distinguished from each other in this Northern blot. The blots were also hybridized with a β-actin control probe to ensure that each tissue samples contained equal amounts of mRNA (data not shown).

The expression pattern of MIM in developing mouse embryos was studied in more detail by RNA *in situ* hybridizations. During development (E10.5–18.5) the strongest MIM expression was in the developing heart, skeletal muscle, and central nervous system (Fig. 3*A* and data not shown). Weak expression was detected in the liver, kidney, and lung (Fig. 3*A* and data not shown). A control hybridization carried out with the sense probe showed that the signal was specific for the MIM mRNA (Fig. 3*B*). Additional hybridizations on mouse embryo sections from various developmental stages demonstrated that MIM is highly expressed in the postmitotic neurons of the spinal cord and brain (Fig. 3, *C* and *E*). Strong expression could also be detected in somitic and migrating myoblasts (Fig. 3*C*), in the developing muscles of the limbs and the body (Fig. 3, *C* and F), and in the developing cardiomyocytes (Fig. 3*D*). Weak expression was detected in the developing sensory systems including the inner ear and eye (Fig. 3*E* and data not shown).

We also examined MIM expression in adult mouse tissues by *in situ* hybridizations. Whereas MIM is strongly and widely expressed in the developing central nervous system until birth, in the adult brain MIM is expressed at high levels only in one special neuronal cell type: the Purkinje cells of the cerebellum (Fig. 3*G*). Weak expression was detected in other parts of the brain such as the septum, the piriform cortex, and the ependymal cells lining the ventricles (data not shown). In the kidney, MIM was highly expressed in the outer medullary zone and weakly in the cortex. MIM expression could not be detected in the medullary inner zone (Fig. 3*H*). Taken together, these hybridizations show that MIM is strongly expressed in the

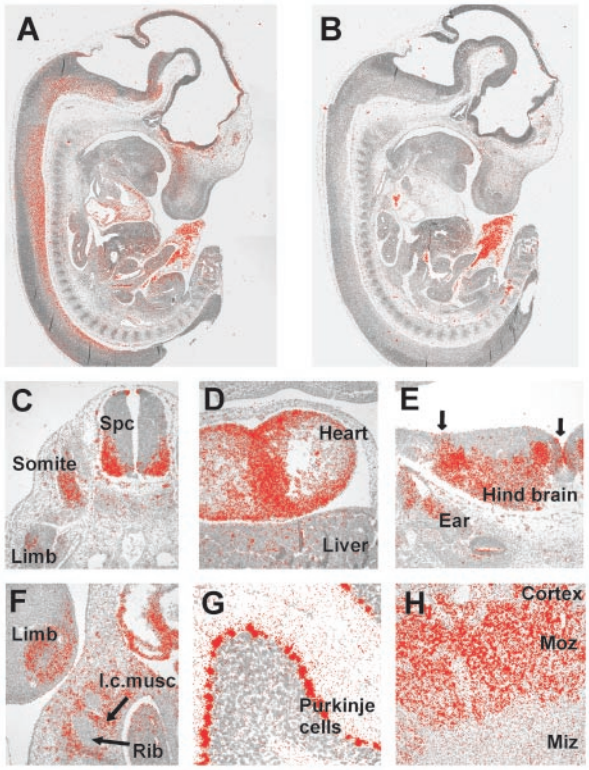

FIG. 3. **An *in situ* hybridization analysis of the MIM expression in mouse embryos and in adult mouse brain and kidney.** *A*, *in situ* hybridization on a sagittal section of an E12.5 embryo with an antisense probe. The expression of MIM is particularly strong in the central nervous system and heart. Weak expression in several inner organs can also be detected. *B*, hybridization of an adjacent section with a control sense probe. Note, that blood cells give some background activity for example in the umbilical cord. *C*, a cross-section through an E11.5 embryo. MIM is expressed in postmitotic neurons of the spinal cord (*spc*), somitic, and migrating myoblasts, and in the developing muscles of the limb. *D*, at E11.5 MIM is strongly expressed in the developing heart and weakly expressed in liver. *E*, cross-section of the mouse hindbrain at E12.5. Strong MIM expression is detected in the differentiating postmitotic neurons. Weak expression can be observed in small populations of proliferating neural precursor cells lining the ventricle (*arrows*) and in the developing inner ear. *F*, at E12.5 high levels of MIM mRNA can be detected in limb and intercostal muscles (*i.c.musc*). No expression can be observed in the developing rib bones. *G*, in the adult mouse brain, MIM expression was detected in the Purkinje cells of the cerebellum. *H*, in adult mouse kidney, MIM expression is restricted to the medullary outer zone (*moz*) and cortex. MIM expression was not detected in the medullary inner zone (*miz*).

developing neurons and muscle cells but is down-regulated during the maturation of these cells. In adult mice MIM is highly expressed only in kidney, liver, and in specialized neuronal cells such as Purkinje cells.

MIM Binds ATP-Actin Monomers through Its C-terminal WH2 Domain—The mouse and human MIM proteins contain a putative actin monomer-binding motif, WH2 domain, in their C termini. To examine whether mouse MIM is an actin-binding protein, we carried out a biochemical characterization of this protein. Because our attempts to express and purify the full-length mouse MIM were unsuccessful, we decided to express the WH2 domain containing C-terminal half (residues 404–759) of the more abundant splice variant of MIM (Fig. 1*A*). This fragment (MIM-CT) was produced as a GST fusion protein in *E. coli*. The GST was removed by thrombin digestion, and recombinant MIM-CT was further purified by anion exchange chromatography.

The fluorescence of the NBD-labeled actin monomers is affected upon interaction with many proteins, including ADF/cofilin, twinfilin, thymosin-β4, and ciboulot, thereby providing

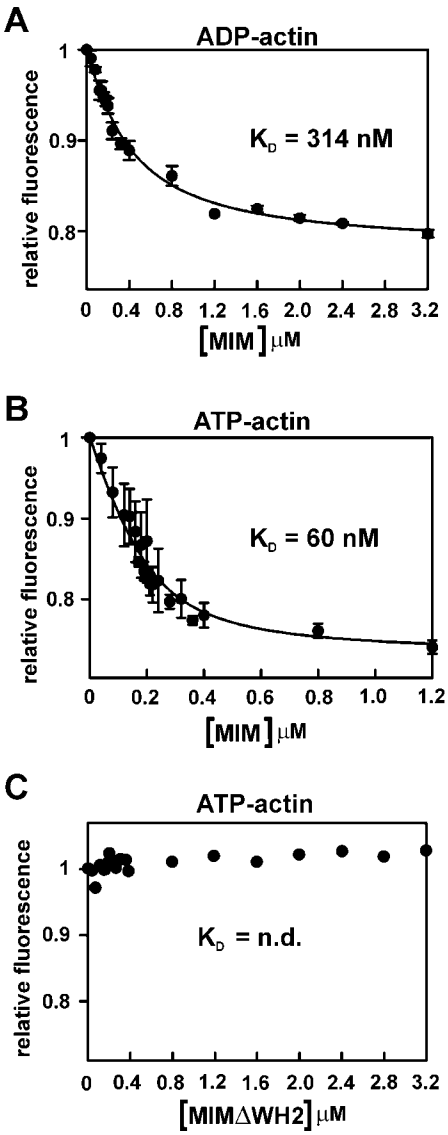

FIG. 4. **Interaction of MIM-CT and MIM-CTΔWH2 with actin monomers.** The change in the fluorescence of 0.2 μM NBD-labeled MgADP-G-actin (*A*) or MgATP-G-actin (*B*, *C*) was measured at different concentrations of MIM-CT under physiological ionic conditions at pH 8.0. *Symbols* are data, and *lines* are the calculated binding curves. Each data point on *graphs A* and *B* is the mean of three independent experiments, whereas the data in *graph C* are from one experiment. Dissociation constants (K_D) derived from the binding curves are indicated in the figure. The MIM-CTΔWH2 protein did not affect NBD-actin fluorescence in this assay, indicating that it does not bind actin monomers with a detectable affinity.

a method to determine the affinities of these proteins for actin monomers (29–31). MIM-CT induced a 20–25% decrease in the fluorescence of NBD-G-actin (Fig. 4). The extent of the NBD-actin fluorescence decrease displayed a saturating behavior enabling us to calculate the K_D values for MIM-CT/actin monomer complexes. MIM-CT bound to both ADP- (Fig. 4*A*) and ATP-actin monomers (Fig. 4*B*) with high affinity. However, the affinity of MIM-CT for ATP-actin monomers was 5-fold higher, (K_D = 0.06 μM) than for ADP-actin monomers (K_D = 0.3 μM). The assay was carried out in physiological ionic conditions (0.1 M KCl, 2 mM $MgCl_2$).

To examine the role of the C-terminal WH2 domain for actin monomer-binding, we designed a mutant protein, MIM-CTΔWH2, in which the WH2 domain was inactivated. The actin-binding site in the WH2 domain of thymosin-β4 has been mapped by mutational studies (28). We constructed a mutant

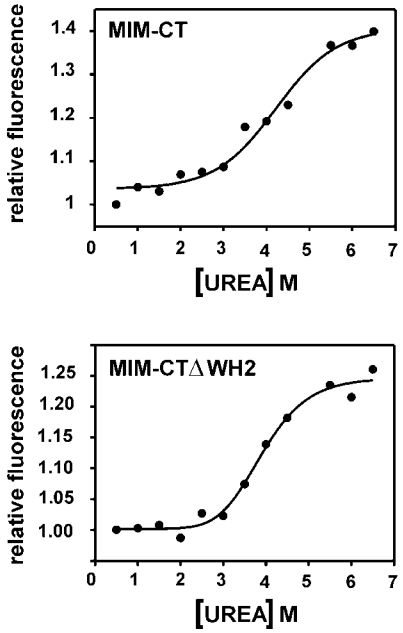

FIG. 5. **The stability of wild-type and mutant MIM-CT proteins measured by fluorescence monitored urea denaturation assay**. The arbitrary fluorescence units are shown on the *y*-axis, and the urea concentration is shown on the *x*-axis. Both the wild-type MIM-CT and MIM-CTΔWH2 unfold at ~4 M urea.

protein in which the corresponding residues (Lys-746 and Lys-747) that have been shown to be most critical for G-actin binding in thymosin-β4 were replaced by alanines, and the last 11 amino acids (749–759) were deleted. The mutant protein was purified as described for wild-type MIM-CT. It showed similar stability than the wild-type MIM-CT in a fluorescence-monitored urea denaturation assay, suggesting that these mutations do not affect the protein stability (Fig. 5). MIM-CTΔWH2 did not affect the fluorescence of NBD-G-actin, suggesting that this mutant protein does not bind actin monomers with a detectable affinity (Fig. 4*C*).

Mouse MIM Inhibits the Nucleation of Actin Filaments, but Its Complex with ATP-G-actin Can Participate in Filament Barbed End Growth—The effect of MIM-CT on actin dynamics was examined by steady-state and kinetic assembly assays. The steady-state assay was an actin filament co-sedimentation assay where the actin concentration was 2 μM and the concentration of MIM-CT was varied from 0 to 4 μM. In the absence of MIM, a majority of actin was present in the pellet fraction, whereas in the presence of 2 and 4 μM MIM-CT ~75% of the actin was shifted to the supernatant fraction. This shows that mouse MIM efficiently decreases actin filament assembly (Fig. 6*A*, *upper panel*). In a similar assay MIM-CTΔWH2 did not increase the amount of monomeric actin, demonstrating that the C-terminal WH2 domain is essential for the ability of MIM to inhibit steady-state F-actin assembly (Fig. 6*A*, *lower panel*). We also carried out an actin filament co-sedimentation assay to examine the interaction of MIM with F-actin. In this assay we used a constant concentration of MIM-CT (2 μM) and varied the concentration of actin from 0 to 8 μM. MIM-CT did not co-sediment with actin filaments, suggesting that MIM does not interact with F-actin with a detectable affinity (data not shown).

Pyrene actin assembly assays were carried out to directly analyze the effects of MIM on actin filament polymerization and nucleation. We first followed the polymerization of 3 μM actin (in the presence of 0/0.75/3 μM MIM-CT or MIM-CTΔWH2) for 10 min after addition of polymerization salts. The data showed that wild-type MIM-CT efficiently inhibits

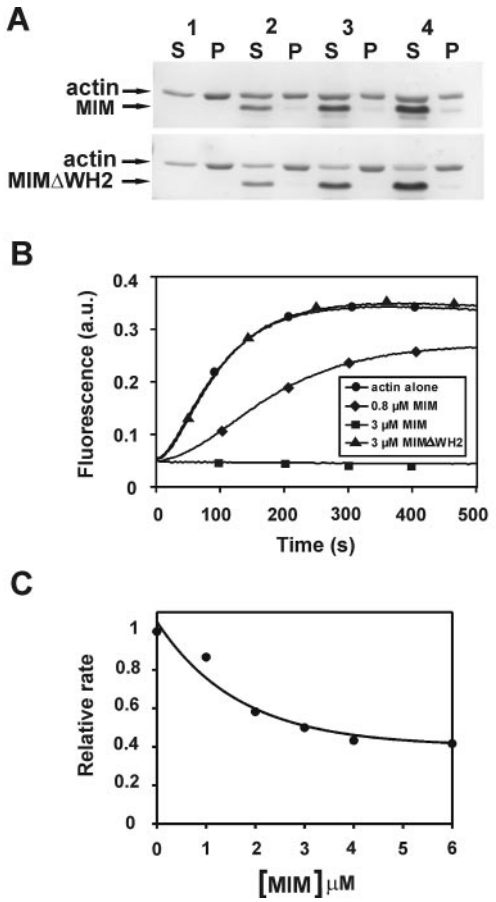

FIG. 6. **Effects of MIM-CT on actin filament nucleation and assembly.** *A*, MIM-CT increases the amount of monomeric actin in an actin filament sedimentation assay (*upper panel*), but MIM-CTΔWH2 does not affect actin sedimentation (*lower panel*). Platelet actin filaments (2 μM) were incubated with 0 (*lane 1*), 1 (*lane 2*), 2 μM (*lane 3*), and 4 μM (*lane 4*) MIM-CT or MIM-CTΔWH2 for 30 min, and the filaments were sedimented by centrifugation. *B*, MIM prevents the nucleation of actin filaments. 3 μM pyrene actin (1:5 pyrene actin: human platelet actin) was polymerized in the presence of 0, 0.8, or 3.0 μM MIM-CT or 3.0 μM MIM-CTΔWH2 by the addition of 0.1 M KCl, 2 mM $MgCl_2$, and 0.5 mM ATP. The polymerization of filaments was followed by the increase in pyrene fluorescence. Wild-type MIM-CT efficiently prevents actin filament assembly, whereas MIM-CTΔWH2 does not have any detectable effect on actin polymerization. *C*, MIM-CT/ATP-G-actin complex can participate in filament barbed end growth. Phalloidin-actin seeds (0.4 μM) were added on a mixture of 3 μM ATP-G-actin and 0/1/2/3/4/6 μM MIM-CT in F-buffer. The polymerization of filaments was followed by the increase in pyrene fluorescence, and the rates were normalized to the rate in the absence of MIM-CT.

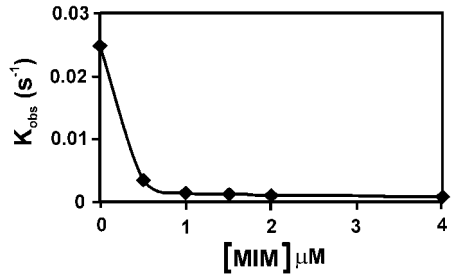

FIG. 7. **MIM-CT inhibits the nucleotide exchange on actin monomer**. The exchange of ϵ-ATP for ATP was monitored by the decrease in the fluorescence at 410 nm. 0.5 μM ϵ-ATP-G-actin was mixed with 0, 0.5, 1, 1.5, 2, or 4 μM MIM-CT, and the decrease in the fluorescence was followed after the addition of 1 mM ATP. The k_{obs} rates obtained from the data are plotted in the graph.

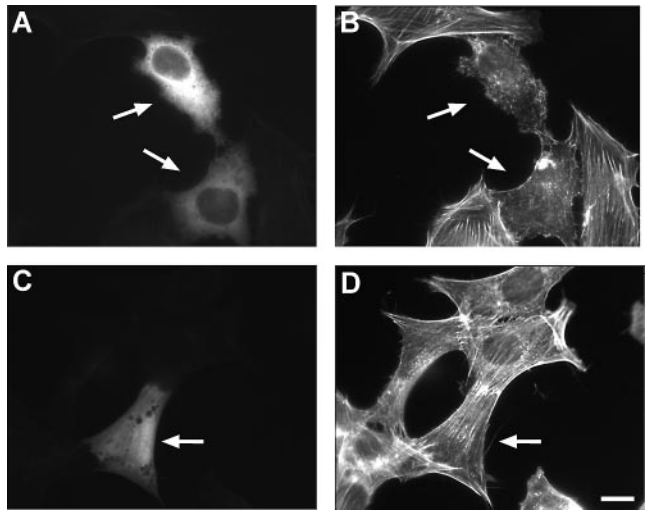

FIG. 8. **Over-expression of MIM results in the formation of abnormal actin filament structures in NIH-3T3 cells.** Cells were transfected with a vector expressing MIM-GFP fusion protein (*A*, *B*) or GFP as a control (*C*, *D*). Localization of GFP-MIM and GFP are shown in *panels A* and *C*, and the actin filaments are visualized by fluorescein-phalloidin in *panels B* and *D*. The cells overexpressing MIM have less stress fibers than untransfected cells and also show an accumulation of abnormal worm-like actin structures. *Scale bar*, 10 μm.

the nucleation and assembly of the actin filaments, whereas MIM-CTΔWH2 did not affect the nucleation/assembly of actin filaments (Fig. 6*B*). We next examined the effects of MIM-CT on filament pointed end and barbed end assembly by using gelsolin-actin and phalloidin-stabilized actin seeds, respectively. MIM-CT efficiently inhibits actin assembly on 10 nM gelsolin-actin seeds demonstrating that MIM-CT blocks the pointed end filament growth (data not shown). MIM-CT also decreases the rate of actin assembly on phalloidin-actin seeds, but even high concentrations of MIM-CT (2-fold molar excess to ATP-G-actin) do not completely block the assembly. Instead, the assembly rate of MIM-CT/ATP-G-actin complex appears to saturate to ~40% level of that of ATP-G-actin alone (Fig. 6*C*). In conclusion, these assays demonstrate that mouse MIM efficiently inhibits the nucleation and pointed end assembly of actin filaments, but its complex with ATP-G-actin can participate in filament barbed end growth. The participation of MIM-CT in barbed end elongation is also in agreement with the co-sedimentation assay (Fig. 6*A*) where MIM-CT, despite its very high affinity for ATP-G-actin (0.06 μM; Fig. 4*B*), was unable to shift all actin to the monomeric fraction even when present in 2-fold molar excess to actin.

MIM Inhibits the Nucleotide Exchange on G-actin—Many actin monomer-binding proteins, such as ADF/cofilin, twinfilin, ciboulot, and thymosin-β4, decrease the rate of nucleotide exchange on actin monomers (31–34). On the other hand small actin monomer-binding protein, profilin, catalyzes the nucleotide exchange on actin monomers (35). We examined the effects of mouse MIM on the nucleotide exchange by following the rate of replacement of ϵ-ATP by ATP on actin monomers in the absence and presence of MIM-CT. MIM inhibits the rate of nucleotide exchange on actin monomers in a concentration-dependent manner (Fig. 7). The inhibition of the nucleotide exchange of 0.5 μM actin is almost saturated already at 0.5 μM MIM-CT. This result is in good agreement with the very high affinity of MIM-CT for ATP-G-actin (0.06 μM, Fig. 4*B*).

Effects of MIM on Actin Dynamics in Vivo—To study the effects of MIM on actin dynamics *in vivo*, we overexpressed mouse MIM as a GFP fusion protein in NIH 3T3 fibroblasts. In the fusion protein constructs GFP was located either at the N terminus or at the C terminus of MIM. In both cases the localization of MIM and the induced phenotypes in cells were

similar to each other, indicating that the GFP did not affect the activity of MIM in cells (data not shown). MIM-GFP fusion proteins were uniformly cytoplasmic in NIH 3T3 cells and not present in the nucleus. Cells over-expressing MIM-GFP showed a clear decrease in the amount of stress fibers and accumulation of abnormal worm-like cytoplasmic actin filament structures (Fig. 8, *A* and *B*). These abnormalities did not occur in untransfected cells or in the cells overexpressing GFP alone (Fig. 8, *C* and *D*). Furthermore, overexpressing MIM-GFP fusion protein in HeLa and NRK cells induced similar abnormalities in the actin cytoskeleton (data not shown). These results suggest that the actin monomer-binding protein MIM is able to regulate actin dynamics also in living cells.

DISCUSSION

We show here that mouse MIM is an actin monomer-binding protein that inhibits the nucleation of actin filaments *in vitro*. These activities reside in the C-terminal WH2 domain of MIM. WH2 domains are also found in many other actin monomer-interacting proteins, such as WASP, Scar, thymosin-β4, ciboulot, actobindin, and WIP/verprolin. All available data indicate that these proteins also interact with actin monomers through their WH2 domains (for recent review see Ref. 5). Furthermore, at least thymosin-β4, ciboulot, and actobindin have significantly higher affinity for ATP-G-actin than for ADP-G-actin (31, 36). Our data shows that mouse MIM affinity for ATP-G-actin is ~5-fold higher than its affinity for ADP-G-actin, suggesting that WH2 domain has evolved as a motif that preferentially binds ATP-G-actin. It is important to note that mouse MIM binds ATP-G-actin with ~20-fold higher affinity (K_D = 0.06 μM, Fig. 4) than thymosin-β4, ciboulot, and actobindin (K_D = 0.7–2 μM) (31). For that reason, we would expect MIM to more drastically affect actin dynamics in cells than for example thymosin-β4.

Most actin monomer-binding proteins, including profilin, ADF/cofilin, twinfilin and WH2 domain proteins bind to the same site on the actin monomer, and thus compete with each other in actin monomer-binding (30, 37–39). Our data show that mouse MIM has a higher affinity for ATP-G-actin (K_D = 0.06 μM) than other actin monomer-binding proteins such as profilin (K_D = 0.1–0.15 μM), ADF/cofilin (K_D = 4–8 μM) and twinfilin (K_D = 0.5 μM) (1, 30). This suggests that in the cells where MIM is expressed, the majority of active MIM is associated with ATP-G-actin. On the other hand, the affinity of mouse MIM for ADP-G-actin (K_D = 0.3 μM), is significantly lower than the ones of ADF/cofilin (K_D = 0.1–0.15 μM) and twinfilin (K_D = 0.05 μM), indicating that MIM would not significantly affect the localization and dynamics of the cellular ADP-actin monomer pool (1, 31).

Some WH2 domain proteins such as thymosin-β4 inhibit actin filament assembly, whereas others such as ciboulot, actobindin and WASP do not sequester actin monomers when the barbed ends of filaments are available (8, 12, 31, 36, 40). Mouse MIM increases the amount of actin monomers in steady-state assembly assays and inhibits actin filament nucleation in kinetic assays (Fig. 6, *A* and *B*). MIM also blocks the pointed end filament assembly, but MIM-CT/ATP-G-actin complexes can participate in barbed end filament elongation (Fig. 6*C*). Therefore, our data suggests that MIM has similar effects on actin assembly as previously described for small WH2 domain proteins cibulot and actobindin (8, 31). However, because MIM is a large, multidomain protein, it is likely to have additional activities that could affect or regulate the actin-modulating activities of the C-terminal WH2 domain.

Our Northern blot and *in situ* hybridization assays demonstrated that MIM mRNA is strongly expressed in developing neurons and myoblasts but absent in most mature neurons and muscle cells. In adult mice, MIM is present in high levels in liver, kidney, and in the cerebellar Purkinje cells (Fig. 3). Similarly, the small actin monomer-sequestering protein, thymosin-β10, is expressed in several developing neuronal cell-types, but only in Purkinje cells in adult animals (41). The transient expression of MIM in developing neurons and myoblasts suggests a role in polarized growth or motility: both processes are actin-dependent and typical for differentiating neurons and myoblasts. Mature muscle cells and neurons lack MIM and have a less dynamic actin cytoskeleton and consequently do not undergo similar morphogenetic changes than their embryonic precursors. The presence of MIM in adult Purkinje cells may be related to the growth and refinement of Purkinje cell dendrites, a phenomenon that probably also takes place in adult animal brains.

It is interesting to note, that the human homologue of MIM was identified as a gene that was present in non-metastatic but absent in metastatic bladder cancer cells (15). Our *in situ* hybridization data show that MIM is strongly expressed in developing neurons and myoblasts (Fig. 3). These are highly polar cell types, suggesting that MIM may help promote and maintain cell polarity. Polarity is essential for the growth and motility of myoblasts and neurons, whereas the loss of polarity in epithelial cells may affect adhesion and precede increased motility, invasiveness, and metastatic capability. This may provide an explanation for the lack of MIM in metastatic bladder cancer cell lines (15). Alternatively, MIM may negatively regulate cytoskeletal dynamics by restricting actin polymerization only to certain regions of migrating cells and in cells that undergo polarized growth. This negative regulatory role is supported by our biochemical (Fig. 6) and cell biological studies, where overexpressing MIM disrupted stress fibers and resulted in formation of abnormal actin filament structures (Fig. 8). In the future it will be important to examine the localization of endogenous MIM protein in various cell types. Unfortunately, our attempts to generate antibodies against mouse MIM have so far been unsuccessful. We would also like to use small interfering RNA and traditional mouse knockout technology to examine the importance of MIM during development and in adult tissues.

Taken together, our data show that mouse MIM binds actin monomers and regulates actin filament assembly in specific polarized mammalian cell-types. Because MIM is a relatively large, multidomain protein, it may have other activities and regulate actin dynamics in a complex fashion. Other large WH2 domain proteins (WASP, Scar, WIP/verprolin) are involved in signaling to the actin cytoskeleton, and the activities of these proteins are regulated by relatively complex mechanisms (1). Therefore, MIM may also be a link between cellular signaling pathways and actin filament assembly. In this respect, it is important to note that MIM contains also several proline-rich motifs that may interact with Src homology 3 or WW domains of certain signaling proteins. In the future it will be important to identify the interaction partners of MIM and learn how they regulate the activity and localization of MIM in specialized mammalian cells.

REFERENCES

1. Pollard, T. D., Blanchoin, L., and Mullins, R. D. (2000) *Annu. Rev. Biophys. Biomolec. Struct.* **29,** 545–576
2. Gimona, M., Djinovic-Carugo, K., Kranewitter, W. J., and Winder, S. J. (2002) *FEBS Lett.* **513,** 98–106
3. Van Troys, M., Vandekerckhove, J., and Ampe, C. (1999) *Biochim. Biophys. Acta* **1448,** 323–348
4. Lappalainen, P. Kessels, M. M., Cope, J. T. V., and Drubin, D. G. (1998) *Mol. Biol. Cell* **9,** 1951–1959
5. Paunola, E., Mattila, P. K., and Lappalainen, P. (2002) *FEBS Lett.* **513,** 92–97
6. Symons, M., Derry, J. M., Karlak, B. J., Jiang, S., Lemahieu, V., McCormick, F., Francke, U., and Abo, A. (1996) *Cell* **84,** 723–734
7. Pantaloni, D., and Carlier, M.-F. (1993) *Cell* **75,** 1007–1014
8. Boquet, I., Boujemaa, R., Carlier, M. F., and Preat, T. (2000) *Cell* **102,** 797–808

9. Machesky, L. M., and Insall, R. H. (1998) *Curr. Biol.* **8,** 1347–1356
10. Higgs, H. N., and Pollard, T. D. (2000) *J. Cell Biol.* **150,** 1311–1320
11. Prehoda, K. E., Scott, J. A., Mullins, R. D., and Lim, W. A. (2000) *Science* **290,** 801–806
12. Yarar, D., D'Alessio, J. A., Jeng, R. L., and Welch, M. D. (2002) *Mol. Biol. Cell.* **13,** 4045–4059
13. Welch, M. D., and Mullins, R. D. (2002) *Annu. Rev. Cell Dev. Biol.* **18,** 247–288
14. Thanabalu, T., and Munn, A. L. (2001) *EMBO J.* **20,** 6979–6989
15. Lee, Y.-G., Macoska, J. A., Korenchuk, S., and Pienta, K. J. (2002) *Neoplasia* **4,** 291–294
16. Peränen, J., and Furuhjelm, J. (2001) *Methods Enzymol.* **329,** 188–196
17. Vartiainen, M., Ojala, P. J., Auvinen, P., Peränen, J., and Lappalainen, P. (2000) *Mol. Cell. Biol.* **20,** 1772–1783
18. Rice, D. B., Aberg, T., Chan, Y., Tang, Z., Kettunen, P. J., Pakarinen, L., Maxon, R. E., and Thesleff, I. (2000) *Development* **127,** 1845–1855
19. Pardee, J. D., and Spudich, J. A. (1982) *Methods Enzymol.* **85,** 164–181
20. Detmers P., Weber A., Elzinga M., and Stephens, R. E. (1981) *J. Biol. Chem.* **256,** 99–105
21. Weeds, A. G., Harris, H., Gratzer, W., and Gooch, J. (1986) *Eur. J. Biochem.* **161,** 77–84
22. Pollard, T. D. (1986) *J. Cell Biol.* **103,** 2747–2754
23. Blanchoin, L., and Pollard, T. D. (1998) *J. Biol. Chem.* **273,** 25106–25111
24. Amann, K. J., and Pollard, T. D. (2001) *Nature Cell Biol.* **3,** 306–310
25. Laemmli, U. K. (1970) *Nature* **227,** 680–685
26. Lappalainen, P., Fedorov E. V., Fedorov, A. A., Almo, S. C., and Drubin, D. G. (1997) *EMBO J.* **16,** 5520–5530
27. Peri, S., and Pandey, A. (2001) *Trends Genet.* **17,** 685–687
28. Van Troys, M., Dewitte, D., Goethals, M., Carlier, M.-F., Vandekerckhove, J., and Ampe, C. (1996) *EMBO J.* **15,** 201–210
29. Carlier, M.-F., Laurent, V., Santolini, J., Melki, R., Didry, D., Xia, G.-X., Hong, Y., Chua, N.-H., and Pantaloni, D. (1997) *J. Cell Biol.* **136,** 1307–1323
30. Ojala, P. J., Paavilainen, V. O., Vartiainen, M. K., Tuma, R., Weeds, A. G., and Lappalainen, P. (2002) *Mol. Biol. Cell* **13,** 3811–3821
31. Hertzog, M., Yarmola, E. G., Didry, D., Bubb, M. R., and Carlier, M. F. (2002) *J. Biol. Chem.* **277,** 14786–14792
32. Hayden, S. M., Miller, P. S., Brauweiler, A., and Bamburg, J. R. (1993) *Biochemistry* **32,** 9994–10004
33. Hawkins, M., Pope, B., Maciver, S. K., and Weeds, A. G. (1993) *Biochemistry* **32,** 9985–9993
34. Goode, B. L., Drubin, D. G., and Lappalainen, P. (1998) *J. Cell Biol.* **142,** 723–733
35. Mockrin, S. C., and Korn, E. D. (1980) *Biochemistry* **19,** 5359–5362
36. Carlier, M.-F., Jean, C., Rieger, K. J., Lenfant, M., and Pantaloni, D. (1993) *Proc. Natl. Acad. Sci. U. S. A.* **90,** 5034–5038
37. Safer, D., Sosnick, T. R., and Elzing, M. (1997) *Biochemistry* **36,** 5806–5816
38. Schutt, C. E., Myslik, J. C., Rozycki, M. D., Goonesekere, N. C., and Lindberg, U. (1993) *Nature* **365,** 810–816
39. Didry, D., Carlier, M. F., and Pantaloni, D. (1998) *J. Biol. Chem.* **273,** 25602–25611
40. Takenawa, T., and Miki, H. (2000) *J. Cell Sci.* **114,** 1801–1809
41. Anadon, R., Moldes, I. R., Carpintero, P., Evangelatos, G., Livianou, E., Leondiadis, L., Quintela, I., Carvino, M. C., and Gomez-Marquez, J. (2001) *Brain Res.* **894,** 255–265